

Spatiotemporal hierarchy of thermal avalanches

Vladimir Yu. Rudyak,¹ Dor Shohat,¹ and Yoav Lahini¹

¹*Department of Condensed Matter, School of Physics and Astronomy, Tel Aviv University, Tel Aviv 69978, Israel*

In amorphous solids, frustrated elastic interactions conspire with thermal noise to trigger anomalously slow sequences of plastic rearrangements, termed "thermal avalanches", which play an important role during creep and glassy relaxations. Here we uncover the complex spatiotemporal structure of thermal avalanches in simulations of a model amorphous solid. We systematically disentangle mechanical and thermal triggering during logarithmic creep, revealing a hierarchy of fast localized cascades linked by slow, long-range, noise-mediated facilitation. These thermal avalanches exhibit heavy-tailed temporal correlations, reminiscent of seismic activity. Our work sheds light on the rich relaxation dynamics of amorphous solids, while providing a framework for identifying noise-mediated correlations. We validate this approach by revealing a similar hierarchy in experiments with crumpled thin sheets.

The dynamics of disordered systems is dominated by intermittent bursts of activity, a hallmark observed across a wide range of systems, from spin glasses [1, 2] and deformed metals [3], through granular and porous materials [4–6], to neuronal activity in the brain [7, 8]. Due to the tendency of disordered systems to lie on the verge of instability [9, 10], an abrupt event – be it a spin flipping, a neuron firing, or a localized plastic deformation – can trigger other events in a rapid sequence, forming an avalanche. These avalanches are typically scale-free and system-spanning [11], and are therefore crucial for the dynamics yet difficult to predict.

Strikingly, avalanche dynamics is strongly altered in the presence of minute temperature or noise. Here, a new triggering mechanism arises, based on facilitation and thermal activation [12–16]. An instability can either trigger the next event immediately; or lower its energy barrier, thus facilitating its stochastic noise-driven activation. Highly correlated sequences of such events, so-called "thermal avalanches", have recently been shown to play a crucial role in the heterogeneous relaxation of glasses [13, 17], and in the creep of amorphous solids [14] and disordered interfaces [18, 19]. Yet, the complex spatiotemporal dynamics they entail remain poorly understood. Gaining insight into these correlations is essential, as they govern how instabilities propagate across disordered systems, ultimately shaping macroscopic phenomena such as slow relaxation, yielding, and flow [20].

In this Letter, we uncover the rich spatiotemporal dynamics of thermal avalanches using simulations of a model amorphous solid – a disordered network of bi-stable elastic bonds [21]. Under an external load and at low temperature, the network exhibits logarithmic creep driven by thermal avalanches [22]. We systematically disentangle their mechanical and thermal components based on correlations in space and time, revealing a complex, hierarchical structure: a localized instability triggers others mechanically, forming fast and compact cascades; each cascade facilitates the thermal activation of the next, giving rise to Omori-like temporal correlations [14, 23, 24] and long-ranged spatial correlations, form-

ing a thermal avalanche; consecutive avalanches exhibit anomalous temporal correlations, akin to those observed between earthquake sequences [25–27]. Finally, we show evidence for this hierarchy in logarithmic creep experiments of crumpled thin sheets [22]. Our study sheds light on the rich dynamics that underly slow relaxations in amorphous solids [14, 28–30], while establishing a framework to identify facilitation-driven correlations and detect thermal avalanches in systems ranging from glass [31, 32] to seismic faults [33, 34].

Disordered network model—We consider a minimal structural model for amorphous solids, a disordered network of $N_b \approx 10^5$ bi-stable elastic springs (Fig. 1a) [21, 35]. Each bond ℓ_i in the network has a double-well potential of the form $U_i(\ell_i) = \frac{a_4}{4}(\ell_i - \ell_i^{(0)})^4 - \frac{a_2}{2}(\ell_i - \ell_i^{(0)})^2$, where the rest length $\ell_i^{(0)}$ is randomized, and a_2, a_4 are network constants (see appendix for details). In the following, we normalize all distances by the mean rest length $\langle \ell^{(0)} \rangle$. Due to the incompatibility between the rest lengths, the bonds carry excess stresses and the network is frustrated. This model was shown to capture several hallmark behaviors of amorphous solids, from memory effects under cyclic driving [36], creep and physical aging [22, 37], to marginal stability [21]. In particular, under an external load and at low temperatures, the network exhibits a slow logarithmic compaction driven by discrete instabilities, abrupt events in which a single bond snaps between the two wells of its potential. These instabilities trigger and facilitate each other, forming scale-free thermal avalanches [14, 22].

We simulate Langevin dynamics of the network using LAMMPS [38], at a very low temperature T and a constant external force F applied at the boundaries, resulting in a slow, intermittent compaction (Fig. 1b). Our simulations track the state of each bond and register the full network configuration only when an instability occurs (see Appendix and [39]). This allows us to track bond snap events with single-time-step accuracy over extremely long simulation times. Below, we leverage this ability to shed light on the complex spatiotemporal dy-

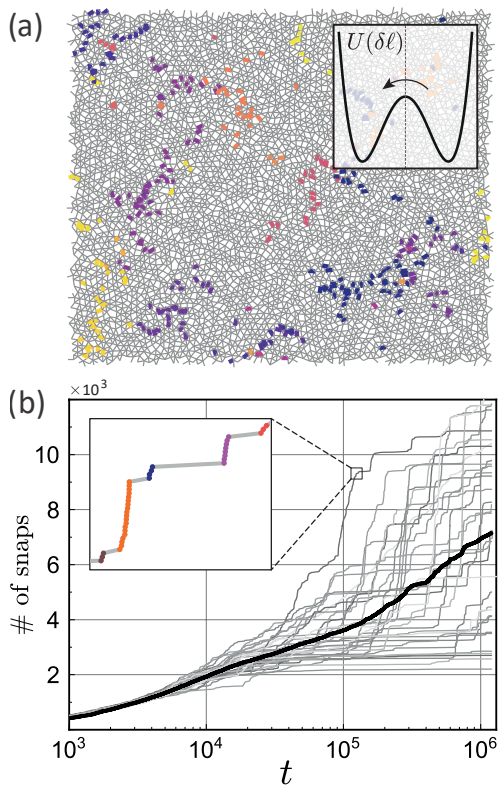


FIG. 1. **Avalanches during creep** – (a) A disordered network of bi-stable bonds (partial view). A single, system spanning thermal avalanche is highlighted, with different colors representing cascades of snaps; Inset: the double-well potential of each bond, as a function of its displacement $\delta\ell = \ell - \ell^{(0)}$; (b) Cumulative number of bond snaps over time for 40 realizations (gray), and their average (black line). The evolution is logarithmic and driven by abrupt avalanches. Inset: Zooming in on a single avalanche reveals distinct cascades.

namics of thermal avalanches.

Elementary instabilities—The first sign of hierarchy in the dynamics is observed in the distribution of waiting times between subsequent bond snaps $P(\Delta t_i = t_i - t_{i-1})$ (Fig. 2, top), calculated at different ages of the system, defined as the time elapsed since the beginning of the experiment. We find that for short waiting times $\Delta t_i < 10$, the distribution is flat and age-independent. In contrast, the long-time behavior slows with the system’s age as longer waiting times are observed. As we show below, these distinct behaviors are associated with different triggering mechanisms.

To distinguish the different mechanisms, we also consider spatial correlations and examine the spatiotemporal distribution of subsequent snaps $P(\Delta t_i, \Delta r_i)$, where $\Delta r_i = |\mathbf{r}_i - \mathbf{r}_{i-1}|$ is the distance between the snapping bonds. We find three regimes shown in Fig. 2: direct mechanical triggering, thermally correlated snaps, and uncorrelated snaps. First, short waiting times $\Delta t_i < \tau_c = 10$ and distances $\Delta r_i < R_c$ ($R_c \approx 40$ bond lengths)

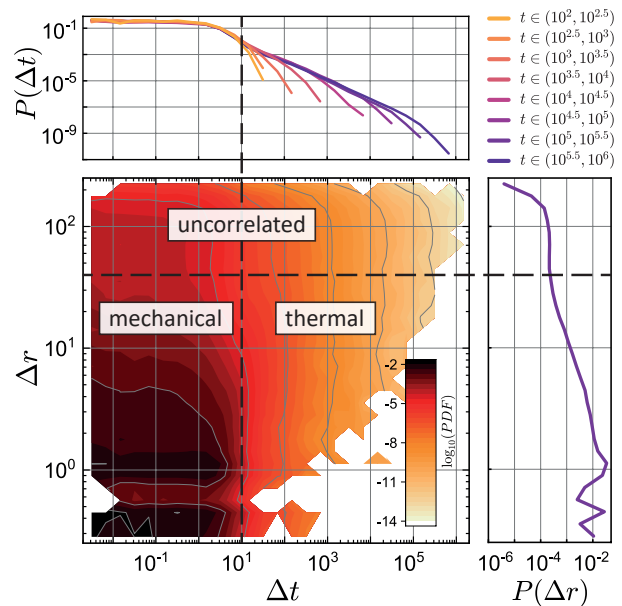


FIG. 2. **Spatiotemporal correlations** – Joint probability distribution $P(\Delta t, \Delta r)$ of the waiting times and distances between consecutive events, divided to three regimes (main panel). The overall distribution of waiting times (top panel) distinguishes between mechanical triggering at short times, and age-dependent thermal triggering at long times. The overall distribution of distances identifies the spatial correlation length R_c .

represent an immediate destabilization of a bond due to the previous bond snap nearby [21]. As noted above, this mechanical triggering is age-independent. Second, longer waiting times $\Delta t_i > \tau_c$ arise from facilitation and thermal activation. Namely, the stress redistribution induced by a snapping bond can lower the energy barrier of other bi-stable bonds, which do not snap immediately but become more prone to thermal activation [12]. These thermal correlations slow down with the age of the system, indicating a gradual increase of the effective energy barriers [14]. Finally, above the correlation length R_c , $P(\Delta r_i)$ reaches the background noise plateau, indicating uncorrelated activity. Having mapped these three regimes, we are now ready to construct a bottom-up understanding of thermal avalanches.

Athermal cascades—We start by characterizing the fast sequences of mechanically triggered snaps, which we term cascades. Scanning all events one by one, a snap is added to the spatially closest cascade that contains a preceding snap with $\Delta t_i < \tau_c$ and $\Delta r_i < R_c$. Otherwise, the snap is considered the first in a new cascade. This process groups snaps into a multitude of cascades that can coexist in different regions of the network. An example of such separation is shown in Fig. 1. The magnitude of each cascade S_c , defined as the number of snaps it contains, is approximately power-law distributed $P(S_c) \sim S_c^{-\alpha}$ with $\alpha \approx 2$ (Fig. 3a).

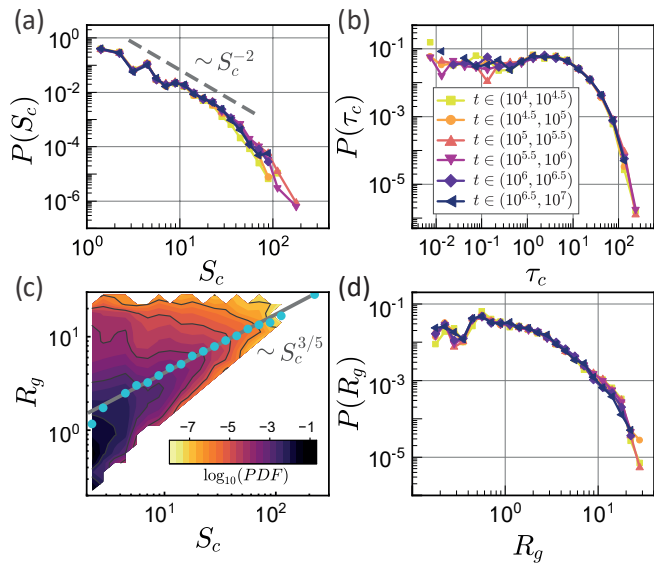


FIG. 3. **Mechanical cascades** – (a) Distribution of cascade magnitudes S_c exhibiting a power law; (b) Distribution of cascade durations τ_c , which is age-independent; (c) Distribution of radii of gyration R_g as a function of S_c , and their mean (teal points); (d) R_g probability distribution.

Next, we compute the duration of each cascade τ_c , the time elapsed between the first and last snaps. We find that the duration distribution $P(\tau_c)$ is compact and age-independent (Fig. 3b).

Spatially, we observe that some cascades are line-like while others resemble more compact blobs (see SI). To characterize these structures, we compute the radius of gyration $R_g^2 = \frac{1}{S_c} \sum_{i=1}^{S_c} (\mathbf{r}_i - \mathbf{r}_{\text{CM}})^2$, where \mathbf{r}_{CM} is the center of mass of the cascade. On average, we find a scaling of $R_g \sim S_c^{3/5}$ (Fig. 3c-d) [40]. Together, these measurements are consistent with the notion that cascades are driven by local mechanical destabilization, which is age-independent.

Thermal avalanches—Taking the next step up the hierarchy, we now consider the slow, thermally correlated activations of events. Here, an event does not trigger the next one immediately. Rather, due to long-range elastic interactions [21], it lowers the energy barriers of other events, thereby facilitating their thermal activation (which can nevertheless occur at a much later time). Such events exhibit long-time correlations, as well as aging due to the growth of these energy barriers [14]. Since mechanical triggering is local and age independent, we can simplify the analysis by considering the spatiotemporal correlations between cascades. To this end, we coarsen cascades to point events in time (using the median time t^{med}) and space (center of mass \mathbf{r}_{CM}). Indeed, the distribution of waiting times between cascades $P(\Delta t^{\text{med}})$, shown in Fig. 4b, captures the age-dependent, power-law tail observed at the single snap level in Fig. 2.

To group cascades into avalanches and determine the

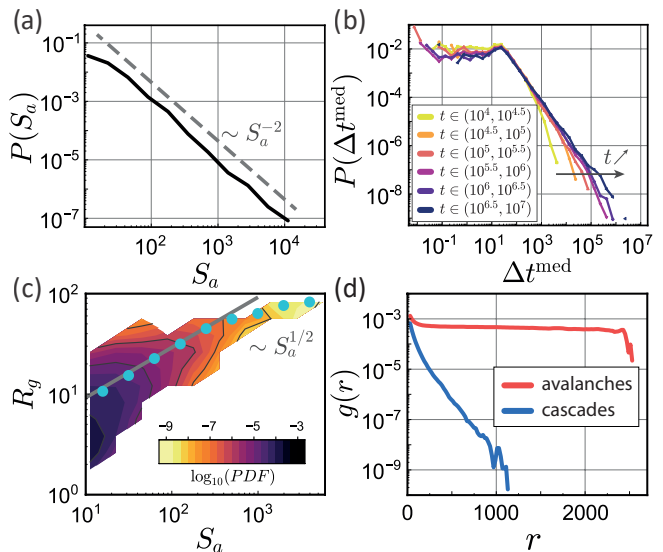


FIG. 4. **Thermal avalanches** – (a) Distribution of avalanche magnitudes S_a exhibiting a power law; (b) Distribution of waiting times between cascades Δt^{med} , with a power-law tail that extends and exhibits aging; (c) Distribution of radii of gyration R_g as a function of S_a , and their mean (teal points); (d) Radial distribution function $g(r)$ for both cascades and avalanches. Cascades are localized while avalanches span the whole network.

spatiotemporal correlations between them, we use an algorithm similar to the one described above for single snaps. However, since the network exhibits aging, and the typical waiting time between correlated cascades grows linearly in time [14, 22], we must consider a varying timescale. Thus, we consider two subsequent cascades as part of the same avalanche if $\Delta(\log t^{\text{med}}) = \log t_i^{\text{med}} - \log t_{i-1}^{\text{med}} < \Theta$ and $\Delta r_{\text{CM}} < R_a$, where Θ is a constant above which the correlation drops sharply (see SI). Here we use the same spatial correlation length $R_a \sim 40$ bond lengths [41]. Additionally, to reduce noise, we ignore cascades that consist of a single snap.

The resulting avalanche magnitudes S_a , representing the total number of snaps, are power law distributed with a similar exponent to the cascade magnitudes $P(S_a) \sim S_a^{-2}$ (Fig. 4a). Yet, in contrast to cascades, thermal avalanches are not compact; an avalanche of magnitude S covers a larger area than that of a single cascade of the same magnitude (see radii of gyration R_g in Figs. 3c and 4c). R_g scales with the avalanche magnitude as $R_g \sim S_a^{1/2}$, before reaching system size. This implies a fractal dimension of approximately $d_f \approx 2$ for large avalanches, consistent with previous work [13] (see SI). To demonstrate that avalanches are system-spanning, we also show the radial distribution function $g(r) = \frac{1}{2\pi r \rho} \langle \sum \delta(\mathbf{r} - \mathbf{r}_i) \rangle$, where ρ is the mean number of snaps per area (Fig. 4d).

Temporal hierarchy—The temporal hierarchy of me-

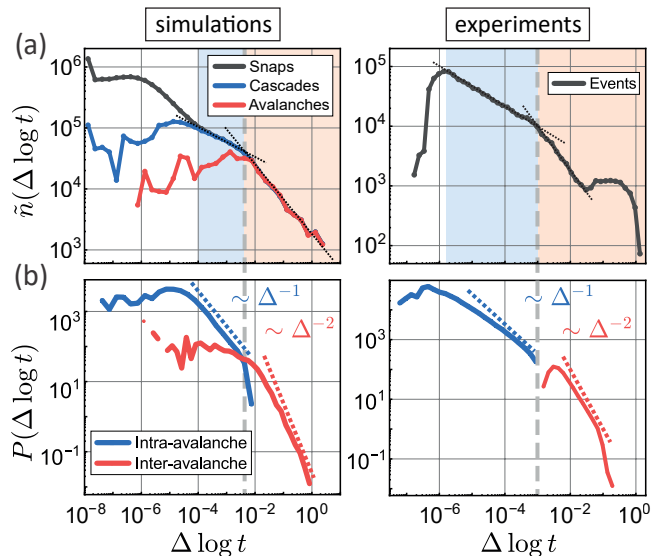


FIG. 5. **Temporal hierarchy** – (a) Conditional event rate \tilde{n} as a function of the log-waiting time, with two regimes representing cascades and avalanches in simulations (left). The same regimes are identified in the experimental data of Ref. [22] (right); (b) Probability distribution of log-waiting times, where power laws $\sim \Delta^{-1}$ and $\sim \Delta^{-2}$ characterize intra- and inter-avalanche activity, respectively.

chanical and thermal correlations is most clear when one analyzes the conditional snap density in log-time $\tilde{n}(\Delta \log t) = \langle n(\log t, \log t + \Delta \log t) | \text{event at } t \rangle$, where n is the number of snaps at a given interval. Fig. 5a, left shows a clear distinction between the three regimes, corresponding to intra-cascade, inter-cascade (intra-avalanche) and inter-avalanche dynamics. The latter two exhibit clear power-law decays, while the transition between them marks the constant Θ defined above. Furthermore, the hierarchy is visible when computing $\tilde{n}(\Delta \log t)$ for cascades or for avalanches instead of single snaps.

These non-trivial correlations are also apparent in the distributions of log waiting times $\Delta \log t = \log t_i - \log t_{i-1}$ (Fig. 5b, left). Within avalanches, the distribution of waiting times between cascades exhibits a power law $P(\Delta \log t) \sim (\Delta \log t)^{-\alpha}$ with $\alpha \approx 1$. Ref. [14] predicted this scaling for thermally activated, correlated barrier crossings. Between avalanches, we find a second power law for the waiting time distribution $P(\Delta \log t) \sim (\Delta \log t)^{-\beta}$ with $\beta \approx 2$. Together, the two regimes are reminiscent of the temporal correlations observed between subsequent earthquakes [25–27].

Experimental validation—Finally, we show that the insights gained from our analysis can be applied to creep experiments, in order to reveal complex correlations as predicted above. To this end, we revisit the results of Refs. [14, 22], which considered the logarithmic compaction of crumpled thin sheets of Mylar under a con-

stant external load. This process was shown to be driven by thermal avalanches of discrete snap-trough instabilities, which could be individually identified using acoustic emission measurements [42–45].

We compute the conditional event rate in log-time for sequences of instabilities during logarithmic relaxation (Fig. 5a, right). Similarly to the model, we find a clear transition between two regimes characterized by different power laws (ultimately reaching a flat background noise level). Following this analogy, the transition clearly identifies a scale Θ^{exp} in log-time that allows separating intra- and inter-avalanche activity.

Using this scale, we define an avalanche S_a^{exp} as a sequence of events with $\Delta \log t < \Theta^{\text{exp}}$ (see SI). To reduce noise, we ignore small avalanches of magnitude $S_a^{\text{exp}} \leq 2$. The log waiting times statistics within and between avalanches, are distributed as power laws with exponents ≈ -1 and ≈ -2 respectively (Fig. 5b, right). While the former scaling distribution was previously reported [14], the latter is much more sensitive to the chosen value of Θ^{exp} , thus demonstrating the strength of our analysis in revealing nontrivial correlations.

Discussion—We studied the spatiotemporal structure of thermal avalanches during logarithmic creep. By examining correlations in space and time as well as the age-dependence of different behaviors, we showed how to systematically distinguish mechanical and thermal contributions. This revealed a hierarchical structure: fast and compact mechanical bursts that facilitate each other’s thermal activation, forming anomalously slow, system-spanning thermal avalanches. It is interesting to compare our results with the relaxation dynamics of glasses, so-called dynamical heterogeneities [46]. Refs. [47, 48] observed a similar hierarchy of relaxation events that cluster both locally and globally. This hints to a potentially deeper connection between logarithmic creep in amorphous solids and slow relaxations in supercooled liquids and glass [13, 14, 49].

The waiting time distributions we found (Fig. 5) show a striking similarity to the inter-event time distributions in a wide range of disordered systems, where two power-law regimes were observed [25–27]. Thus, thermal avalanches suggest a potential mechanism for earthquake aftershock triggering [50], as well as the intermittent dynamics during shear and compression of granular materials [51, 52], porous materials [6], or wood [53]. Interpreting the two power-law regimes as intra- and interavalanche correlations may shed light on their origin, as we demonstrated for the crumpled sheet experiments. Finally, our bottom-up recipe for avalanche identification could be relevant for the analysis of earthquake data, where clustering is notoriously difficult [33].

Acknowledgements—We thank Daniel Korchinski, Marko Popović, and Matthieu Wyart for insightful comments. This work was supported by the Israel Science Foundation grant 2117/22. D.S. acknowledges support

from the Clore Israel Foundation. V.R. acknowledges support from The Council of Higher Education and the Ministry of Immigration and Absorption.

Appendix: Numerical simulations

We simulated two-dimensional disordered networks consisting of 4×10^4 nodes of unit mass connected by $N 10^5$ bi-stable elastic bonds. Each bond has double-well potential $U_i(\ell_i) = a_4/4(\ell_i - \ell_i^{(0)})^4 - a_2/2(\ell_i - \ell_i^{(0)})^2$, where ℓ_i is the i^{th} bond's length, $\ell_i^{(0)}$ is its rest length, and $a_2 = 2.5$, $a_4 = 1$ are network constants. The rest lengths were chosen randomly in the range $\ell^{(0)} \in [9, 11]$, resulting in a random disordered network. We use over-coordinated networks with $\Delta Z = Z - Z_c \approx 1.5$, where Z is the mean number of neighbors per node, and Z_c marks the isostatic point. More details on the network topology and its preparation can be found in Ref. [36].

Molecular dynamics was simulated in the canonical ensemble. An additional 12/6 Lennard-Jones potential with $\varepsilon_{LJ} = 10$ and $\sigma_{LJ} = 11.2246$ was introduced between pairs of non-neighboring nodes to avoid phantom behavior of the network. We use a Langevin thermostat at temperature $T = 0.001$, and damping time $\tau_{damp} = 4$. All simulations were performed in LAMMPS [38] with modified `bond_bpm`, `bond_bpm_spring`, and `bond_table` modules, which implement precise logging of bond snap events. Modified LAMMPS modules, and an example run script and output are available for download [39], see SI for details.

To detect bond snapping, each bond potential was divided into three regions, or states: ‘short’ ($\ell_i - \ell_i^{(0)} \leq -0.7$), ‘transition’ ($-0.7 < \ell_i - \ell_i^{(0)} \leq 0.3$), and ‘long’ ($\ell_i - \ell_i^{(0)} > 0.3$). The simulation tracks the state of each bond in the current time step, its state in the previous time step, and the last state different from the previous one (i.e. the state from which it came to the state at the previous timestep). We define a bond snap as a sequence of transitions from ‘long’ to ‘transition’ to ‘short’ or *vice versa*, but not ‘long’ to ‘transition’ to ‘long’ or ‘short’ to ‘transition’ to ‘short’. In other words, a bond is considered to snap, when its current state is ‘long’ (‘short’), the previous state is ‘transition’, and the state before that is ‘short’ (‘long’). Importantly, this instability tracking is done entirely on the fly in LAMMPS via the specific modules listed above, and does not require post-analysis of a stepwise trajectory. A graphical representation of the snap analysis is shown in the SI.

The initial network was prepared by the following equilibration procedure. First, the system was equilibrated without external stress at temperature $T = 1$, which is high enough to overcome the bi-stable bond barrier and thus randomize states of all bonds. Second, the systems was gradually cooled to $T = 0.001$ in 3×10^4 time units

and then equilibrated at this temperature for 3×10^4 time units more to ensure the absence of bond snaps at low temperature.

To implement external stress conditions, a force $F = 0.61$ acted on the boundaries of the network. Relaxation of the system under stress was simulated for 6×10^6 time units in 20 independent trajectories. In addition, 20 shorter simulations of 1.2×10^6 time units were performed for improved statistics results at shorter times. For every trajectory, the configuration of the network was written after each bond snap, allowing a detailed analysis of the deformation process.

-
- [1] O. Perković, K. Dahmen, and J. P. Sethna, Avalanches, barkhausen noise, and plain old criticality, *Physical review letters* **75**, 4528 (1995).
 - [2] F. Pázmándi, G. Zaránd, and G. T. Zimányi, Self-organized criticality in the hysteresis of the sherrington-kirkpatrick model, *Physical review letters* **83**, 1034 (1999).
 - [3] J. Antonaglia, W. J. Wright, X. Gu, R. R. Byer, T. C. Hufnagel, M. LeBlanc, J. T. Uhl, and K. A. Dahmen, Bulk metallic glasses deform via slip avalanches, *Physical review letters* **112**, 155501 (2014).
 - [4] B. Shang, P. Guan, and J.-L. Barrat, Elastic avalanches reveal marginal behavior in amorphous solids, *Proceedings of the National Academy of Sciences* **117**, 86 (2020).
 - [5] D. Denisov, K. Lőrincz, J. Uhl, K. A. Dahmen, and P. Schall, Universality of slip avalanches in flowing granular matter, *Nature communications* **7**, 10641 (2016).
 - [6] J. Baró, Á. Corral, X. Illa, A. Planes, E. K. Salje, W. Schranz, D. E. Soto-Parra, and E. Vives, Statistical similarity between the compression of a porous material and earthquakes, *Physical review letters* **110**, 088702 (2013).
 - [7] J. M. Beggs and D. Plenz, Neuronal avalanches in neocortical circuits, *Journal of neuroscience* **23**, 11167 (2003).
 - [8] N. Friedman, S. Ito, B. A. Brinkman, M. Shimono, R. L. DeVille, K. A. Dahmen, J. M. Beggs, and T. C. Butler, Universal critical dynamics in high resolution neuronal avalanche data, *Physical review letters* **108**, 208102 (2012).
 - [9] M. Müller and M. Wyart, Marginal stability in structural, spin, and electron glasses, *Annu. Rev. Condens. Matter Phys.* **6**, 177 (2015).
 - [10] J. Lin and M. Wyart, Mean-field description of plastic flow in amorphous solids, *Physical review X* **6**, 011005 (2016).
 - [11] P. Bak, C. Tang, and K. Wiesenfeld, Self-organized criticality: An explanation of the 1/f noise, *Physical review letters* **59**, 381 (1987).
 - [12] M. Ozawa and G. Biroli, Elasticity, Facilitation, and Dynamic Heterogeneity in Glass-Forming Liquids, *Phys. Rev. Lett.* **130**, 138201 (2023).
 - [13] A. Tahaei, G. Biroli, M. Ozawa, M. Popović, and M. Wyart, Scaling description of dynamical heterogeneity and avalanches of relaxation in glass-forming liquids, *Physical Review X* **13**, 031034 (2023).
 - [14] D. J. Korchinski, D. Shohat, Y. Lahini, and

- M. Wyart, Microscopic description of the intermittent dynamics driving logarithmic creep, arXiv preprint arXiv:2409.17415 (2024).
- [15] E. E. Ferrero, L. Foini, T. Giamarchi, A. B. Kolton, and A. Rosso, Spatiotemporal patterns in ultraslow domain wall creep dynamics, *Physical review letters* **118**, 147208 (2017).
- [16] B. Guiselin, C. Scalliet, and L. Berthier, Microscopic origin of excess wings in relaxation spectra of supercooled liquids, *Nature Physics* **18**, 468 (2022).
- [17] C. Gavazzoni, C. Brito, and M. Wyart, Testing theories of the glass transition with the same liquid but many kinetic rules, *Physical Review Letters* **132**, 248201 (2024).
- [18] G. Durin, V. M. Schimmenti, M. Baiesi, A. Casiraghi, A. Magni, L. Herrera-Diez, D. Ravelosona, L. Foini, and A. Rosso, Earthquake-like dynamics in ultrathin magnetic films, *Physical Review B* **110**, L020405 (2024).
- [19] T. W. De Geus, A. Rosso, and M. Wyart, Dynamical heterogeneities of thermal creep in pinned interfaces, *Physical Review E* **111**, L013503 (2025).
- [20] A. Nicolas, E. E. Ferrero, K. Martens, and J.-L. Barrat, Deformation and flow of amorphous solids: Insights from elastoplastic models, *Reviews of Modern Physics* **90**, 045006 (2018).
- [21] D. Shohat, Y. Lahini, and D. Hexner, Emergent marginality in frustrated multistable networks, *The Journal of Chemical Physics* **162** (2025).
- [22] D. Shohat, Y. Friedman, and Y. Lahini, Logarithmic aging via instability cascades in disordered systems, *Nature Physics* **19**, 1890 (2023).
- [23] T. Senshu, On the time interval distribution of aftershocks, *Zisin, Ser. 2* **12**, 149 (1959).
- [24] P. Bak, K. Christensen, L. Danon, and T. Scanlon, Unified scaling law for earthquakes, *Physical Review Letters* **88**, 178501 (2002).
- [25] A. Corral, Local distributions and rate fluctuations in a unified scaling law for earthquakes, *Physical Review E* **68**, 035102 (2003).
- [26] A. Talbi and F. Yamazaki, A mixed model for earthquake interevent times, *Journal of Seismology* **14**, 289 (2010).
- [27] H. Li, E. Valdés, and E. Vives, Double power-law universal scaling function for the distribution of waiting times in labquake catalogs, *Physical Review E* **110**, 064140 (2024).
- [28] M. Popović, T. W. de Geus, W. Ji, A. Rosso, and M. Wyart, Scaling description of creep flow in amorphous solids, *Physical Review Letters* **129**, 208001 (2022).
- [29] D. Bouttes and D. Vandembroucq, Creep of amorphous materials: A mesoscopic model, in *AIP Conference Proceedings*, Vol. 1518 (American Institute of Physics, 2013) pp. 481–486.
- [30] A. Cottrell, The time laws of creep, *Journal of the Mechanics and Physics of Solids* **1**, 53 (1952).
- [31] H. Bhaumik, G. Foffi, and S. Sastry, Avalanches, clusters, and structural change in cyclically sheared silica glass, *Physical Review Letters* **128**, 098001 (2022).
- [32] Y. Takaha, H. Mizuno, and A. Ikeda, Avalanche criticality emerges by thermal fluctuation in a quiescent glass, arXiv preprint arXiv:2409.15775 (2024).
- [33] I. Zaliapin and Y. Ben-Zion, A global classification and characterization of earthquake clusters, *Geophysical Journal International* **207**, 608 (2016).
- [34] D. Houdoux, A. Amon, D. Marsan, J. Weiss, and J. Crasous, Micro-slips in an experimental granular shear band replicate the spatiotemporal characteristics of natural earthquakes, *Communications Earth & Environment* **2**, 90 (2021).
- [35] L. Yan, G. Düring, and M. Wyart, Why glass elasticity affects the thermodynamics and fragility of supercooled liquids, *Proceedings of the National Academy of Sciences* **110**, 6307 (2013).
- [36] D. Shohat, D. Hexner, and Y. Lahini, Memory from coupled instabilities in unfolded crumpled sheets, *Proceedings of the National Academy of Sciences* **119**, e2200028119 (2022).
- [37] D. Shohat, P. Baconnier, I. Procaccia, M. van Hecke, and Y. Lahini, Aging of amorphous materials under cyclic strain, arXiv preprint arXiv:2506.08779 (2025).
- [38] A. P. Thompson, H. M. Aktulga, R. Berger, D. S. Bolintineanu, W. M. Brown, P. S. Crozier, P. J. In't Veld, A. Kohlmeyer, S. G. Moore, T. D. Nguyen, et al., LAMMPS—a flexible simulation tool for particle-based materials modeling at the atomic, meso, and continuum scales, *Computer physics communications* **271**, 108171 (2022).
- [39] LAMMPS user modules and example files, <https://drive.google.com/drive/folders/1F-TvOnUF383ma8PULHzqoTIDqIsV0gV-?usp=sharing>, [Accessed 18-05-2025].
- [40] The scaling $R_g \sim S_c^{3/5}$ indicates that cascades occupy more space than a standard random walk due to self-avoidance effects.
- [41] Alternatively, choosing a correlation length that grows with the speed of sound in the system yields similar results, as we discuss in the SI.
- [42] D. Shohat and Y. Lahini, Dissipation indicates memory formation in driven disordered systems, *Physical Review Letters* **130**, 048202 (2023).
- [43] Y. Lahini, S. M. Rubinstein, and A. Amir, Crackling noise during slow relaxations in crumpled sheets, *Physical Review Letters* **130**, 258201 (2023).
- [44] E. M. Kramer and A. E. Lobkovsky, Universal power law in the noise from a crumpled elastic sheet, *Physical Review E* **53**, 1465 (1996).
- [45] P. A. Houle and J. P. Sethna, Acoustic emission from crumpling paper, *Physical Review E - Statistical Physics, Plasmas, Fluids, and Related Interdisciplinary Topics* **54**, 278 (1996).
- [46] L. Berthier, G. Biroli, J.-P. Bouchaud, L. Cipelletti, and W. van Saarloos, *Dynamical heterogeneities in glasses, colloids, and granular media*, OUP Oxford **150** (2011).
- [47] R. Candelier, O. Dauchot, and G. Biroli, Building blocks of dynamical heterogeneities in dense granular media, *Physical review letters* **102**, 088001 (2009).
- [48] R. Candelier, A. Widmer-Cooper, J. K. Kummerfeld, O. Dauchot, G. Biroli, P. Harrowell, and D. R. Reichman, Spatiotemporal hierarchy of relaxation events, dynamical heterogeneities, and structural reorganization in a supercooled liquid, *Physical review letters* **105**, 135702 (2010).
- [49] C. Scalliet, B. Guiselin, and L. Berthier, Thirty milliseconds in the life of a supercooled liquid, *Physical Review X* **12**, 041028 (2022).
- [50] J. Weiss and D. Marsan, Thermally activated static friction explains earthquake interactions, preprint (2024).
- [51] S. Lherminier, R. Planet, V. L. D. Vehel, G. Simon, L. Vanel, K. J. Måløy, and O. Ramos, Continuously

- sheared granular matter reproduces in detail seismicity laws, *Physical review letters* **122**, 218501 (2019).
- [52] J. Barés, D. Wang, D. Wang, T. Bertrand, C. S. O'Hern, and R. P. Behringer, Local and global avalanches in a two-dimensional sheared granular medium, *Physical Review E* **96**, 052902 (2017).
- [53] T. Mäkinen, A. Miksic, M. Ovaska, and M. J. Alava, Avalanches in wood compression, *Physical review letters* **115**, 055501 (2015).